IEEE Photonics Journal
An IEEE Photonics Society Publication

Open Access

Improved Optical Properties of Nonpolar AlGaN-Based Multiple Quantum Wells Emitting at 280 nm

Volume 13, Number 1, February 2021

Jianguo Zhao
Jiangyong Pan
Bin Liu, *Senior Member, IEEE*
Tao Tao
Daihua Chen
Xianjian Long
Zhe Chuan Feng
Jianhua Chang

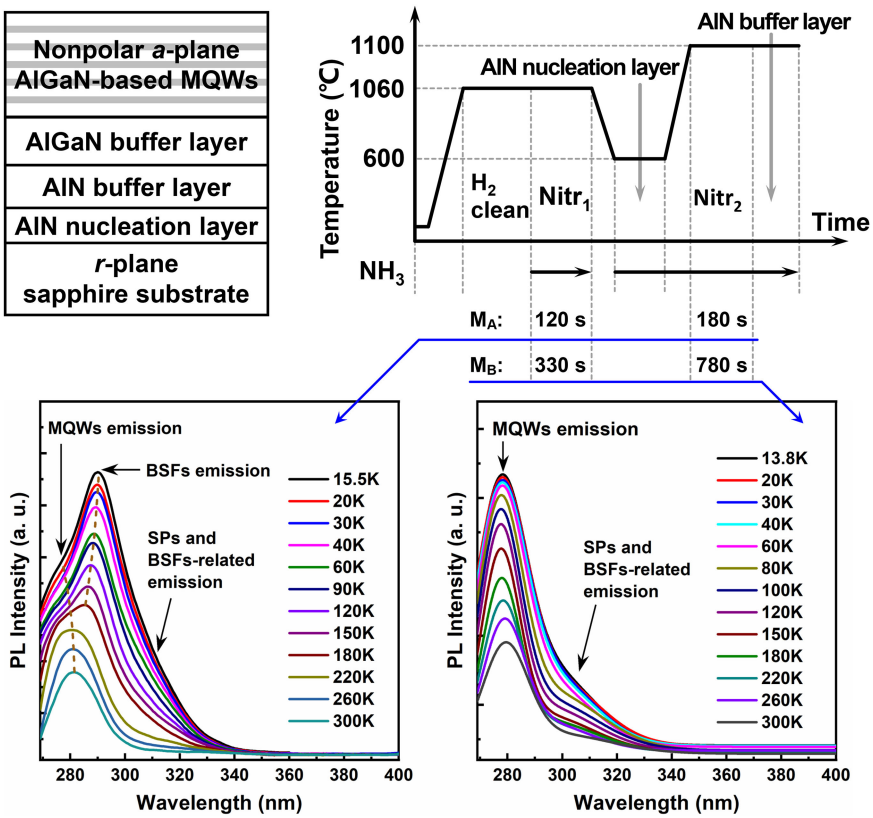

DOI: 10.1109/JPHOT.2020.3039897

Improved Optical Properties of Nonpolar AlGaN-Based Multiple Quantum Wells Emitting at 280 nm

Jianguo Zhao,[1,2] **Jiangyong Pan**,[1] **Bin Liu**,[2] ***Senior Member, IEEE***, **Tao Tao**,[2] **Daihua Chen**,[3] **Xianjian Long**,[3] **Zhe Chuan Feng**,[3] **and Jianhua Chang**[1]

[1]School of Electronic and Information Engineering, Nanjing University of Information Science and Technology, Nanjing 210044, China
[2]School of Electronic Science and Engineering, Nanjing University, Nanjing 210093, China
[3]Laboratory of Optoelectronic Materials & Detection Technology, Guangxi University, Nanning 530004, Guangxi, China

DOI:10.1109/JPHOT.2020.3039897

Manuscript received October 19, 2020; revised November 14, 2020; accepted November 18, 2020. Date of publication November 24, 2020; date of current version December 31, 2020. This work was supported in part by the Startup Foundation for Introducing Talent of NUIST under Grant 2019r036, in part by the Natural Science Foundation of the Jiangsu Higher Education Institutions of China under Grant 19KJB510006, in part by the National Nature Science Foundation of China under Grants 62074077, 61921005, and 61974062, and the China Postdoctoral Science Foundation under Grant 2020M671441. Corresponding author: Bin Liu (e-mail: bliu@nju.edu.cn).

Abstract: The optical properties of nonpolar AlGaN multiple quantum wells (MQWs) emitting at 280 nm were investigated intensively using temperature-dependent and time-resolved photoluminescence spectra associated with the characterization of structural properties. The densities of superficial pits and basal-plane stacking faults (BSFs) were reduced by 33.8% and 35.9%, respectively, for nonpolar AlGaN MQWs due to the carefully optimized dual nitridation. It was found that the nonpolar MQWs emission can be significantly improved by reducing the BSFs density as the BSFs emission was the main competing channels. Moreover, an internal quantum efficiency of 39% for nonpolar $Al_{0.43}Ga_{0.57}N$ MQWs at emission wavelength of 279 nm was achieved even the full width at half maximum values of X-ray rocking curves were 0.565° for *c*-direction and 0.797° for *m*-direction. This fact means that a highly efficient deep ultraviolet light sources can be expected by means of nonpolar AlGaN due to the elimination of quantum confined Stark effect induced the decrease in radiative lifetime.

Index Terms: Deep ultraviolet light source, nonpolar AlGaN-based multiple quantum wells, temperature-dependent and time-resolved photoluminescence, internal quantum efficiency.

1. Introduction

AlGaN-Based ultraviolet and deep-ultraviolet (DUV) light-emitting diodes (LEDs) are the promising semiconductor ultraviolet light sources due to the possibility of achieving efficient ultraviolet light emission from AlGaN-based multiple quantum wells (MQWs), the realizability of N- and P-type semiconductors in DUV spectral region, as well as the steady physical properties and long device lifetime [1]–[4]. In the DUV emission region, the highest external quantum efficiency was reported to be 20.3% at 275 nm achieved by using a serious features such as Rh mirror electrode and AlN template for a flip-chip LED structure [5]. Moreover, a high enhancement in IQE was achieved by

large misoriented sapphire substrate [6] and defect engineering [7]. These achievements are still unsatisfactory compared with the GaN-based blue light counterpart [8]. The development of DUV LEDs was restricted due to the polarization electric field-induced quantum confined Stark effect (QCSE) [9] and the low hole injection efficiency resulted by low hole concentration of P-type AlGaN [1]. Another alternative approach may be to utilize nonpolar AlGaN to achieve high-efficiency DUV LEDs. The extensive study on nonpolar group-III nitrides was started in 2000 and then received much attention as the IQE can be highly improved for the irreplaceable advantage: short radiative lifetime and decreased competing nonradiative recombination due to the elimination of QCSE [10]. Moreover, an enhanced hole concentration in nonpolar P-type AlGaN could be expected according to the reports that the activation energy was more than 30% lower in nonpolar $(11\bar{2}0)$ *a*-plane GaN than that in polar (0001) *c*-plane GaN [11], [12]. Thus, a high speed ultraviolet light communication and large injection current can be expected for a nonpolar AlGaN-based DUV light source. The heteroepitaxy growth of nonpolar *a*-plane GaN and AlGaN on $(1\bar{1}02)$ *r*-plane sapphire substrate has attracted increasing attention since the low cost commercially available sapphire substrate. However, the crystalline quality of nonpolar AlGaN was much poorer than the polar counterpart owing to the anisotropy for both the lattice mismatch and growth velocities between the in-plane *c*- and *m*-directions [13]. Furthermore, the densities of superficial pits (SPs) and basal plane stacking faults (BSFs) in nonpolar AlGaN were usually high and thus resulted in a rough surface morphology. Hence the research progress on nonpolar AlGaN is inferior to that on the conventional polar AlGaN. Until now, there is still no reports on the successful fabrication of nonpolar DUV LEDs. On the other hand, the studies on nonpolar AlN or AlGaN with relatively high Al composition were much less than that on nonpolar GaN as the epitaxial growth of nonpolar AlN and AlGaN epilayers were much more difficult in comparison to GaN. The root-mean-square (RMS) value of nonpolar AlGaN films was generally larger than 10 nm [14], that is too large for further applications, especially to grow MQWs structure. Recently, Jo *et al.* reported the achievement of 2 μm-thick nonpolar AlN layer whose RMS value was only 2.2 nm grown with V/III ratio of 50 at 1500 °C [15]. Meanwhile, by optimizing the pulsed growth method, a nonpolar $Al_{0.68}Ga_{0.32}N$ layer with a RMS of 2.02 nm was reported by our group [14]. However, while the Al composition in nonpolar AlGaN estimated using absorption edge was decreased to 0.54, which is essential for an emission in DUV wavelength, it was found that the measured RMS value had increased to 5.70 nm. Eventually, by introducing trimethyl-aluminum duty-ratio growth method and optimizing dual nitridation process, a high quality nonpolar AlGaN MQWs emitted at 279 nm was successfully grown by our group [16], [17]. Despite the recent achievement on nonpolar AlN or AlGaN, there was yet not intensively studies on nonpolar AlGaN MQWs emitting at DUV region.

In this paper, the optical properties of nonpolar *a*-plane AlGaN MQWs emitting at 280 nm were studied intensively using the temperature-dependent photoluminescence (PL) (TDPL) and time-resolved PL (TRPL) spectra associated with the structural characteristics. It was found that the BSFs emission was the main competing channels for nonpolar AlGaN-based MQWs, and a higher realizability of efficient deep ultraviolet light sources can be expected by means of nonpolar AlGaN than polar counterpart.

2. Experimental

In this study, the nonpolar $(11\bar{2}0)$-plane AlGaN MQWs were grown on 2-inch $(1\bar{1}02)$-plane sapphire substrate with a 40 Torr metal organic chemical vapor deposition system, and the layer structure was demonstrated in Fig. 1(a). The growth temperature, thickness, and V/III ratio of AlN nucleation layer, AlN buffer layer, and AlGaN buffer layer were 600, 1100, and 1100 °C, 30, 120, and 350 nm, and 18000, 2000, and 1000, respectively. Moreover, the AlN and AlGaN buffer layers were grown with a two-way pulsed-flows growth technology [14]. The 5-period of nonpolar AlGaN MQWs were grown with the identical growth method and parameters as our previously reported and the thickness of quantum barriers and quantum wells were confirmed to be 10.5 and 3.9 nm both by the X-ray diffraction (XRD) fitting results and transmission electron microscope (TEM) measurements [16]. Two samples were grown with the identical growth parameters except for the duration of dual

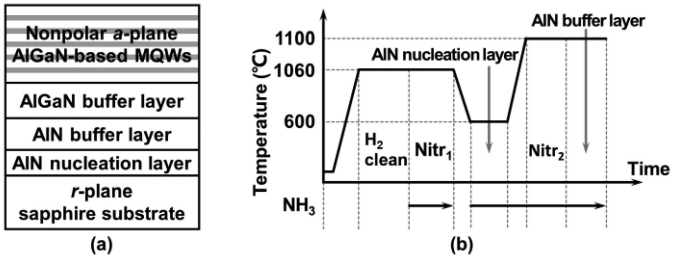

Fig. 1. Layer structure (a) and temperature variation chart in the initial growth process (b) for the nonpolar AlGaN MQWs.

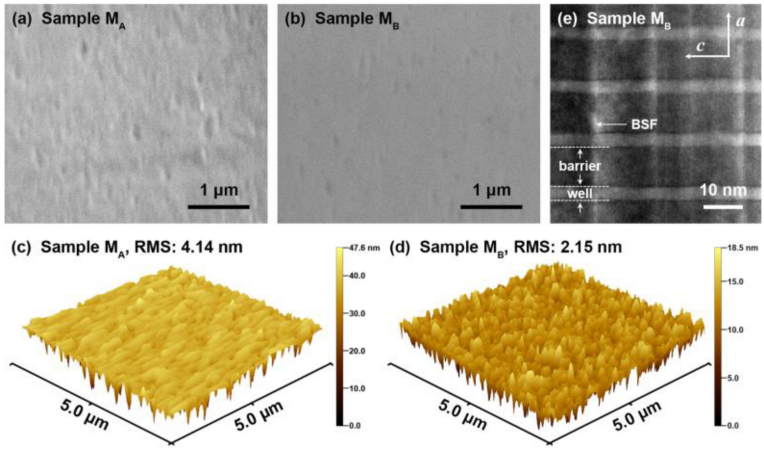

Fig. 2. Surface SEM (a, b) and AFM (c, d) images for samples M_A and M_B; Cross profile TEM image (e) in MQWs area for sample M_B.

nitridation process. Fig. 1(b) demonstrated the temperature variation chart for the initial growth process. The dual nitridation process contained the first nitridation for sapphire substrate and the second nitridation for AlN nucleation layer labeled as $Nitr_1$ and $Nitr_2$, respectively as shown in Fig. 1(b). For sample M_A, the duration for $Nitr_1$ was 120 s and the duration for $Nitr_2$ was 180 s as the necessary temperature stabilization time. For sample M_B, the duration for $Nitr_1$ and $Nitr_2$ was set to be 330 and 780 s, respectively after the careful optimizing [17]. Here, it was worth to note that only the black arrow labeled section as illustrated in the bottom of Fig. 1(b) was fed with ammonia.

After growth, the samples were cut into 1×1 cm^2 for the extensive measurements. TDPL spectra were characterized using a 266 nm pulsed laser with a power density of 2.1×10^5 W·cm^{-2}. TRPL spectra was performed at 13K with a 213 nm laser, whose power density, repetition rate, and pulse duration are 4.5×10^8 W·cm^{-2}, 5 kHz, and 42 picosecond (ps), respectively. The luminescence was collected with Zolix Omni-λ 750i spectrometer and detected with a photomultiplier tube. The TRPL spectra was recorded with PMA 182-N-M photon counter. A Phenom ProX scanning electron microscopy (SEM), Bruker BioScope Resolve atomic force microscope (AFM), and FEI Talos F200S TEM were carried out to evaluate the surface morphologies and cross section of prepared nonpolar MQWs. XRD curves were performed with PANalytical X'pert PRO worked in 'double axis' instrument.

3. Results and Discussions

As demonstrated in Fig. 2(a–d), the surface morphology of both samples M_A and M_B were firstly characterized utilizing SEM and AFM. The SPs distributed on the samples surface were formed because the anisotropy of growth velocities along the various in-plane directions for *a*-plane AlGaN

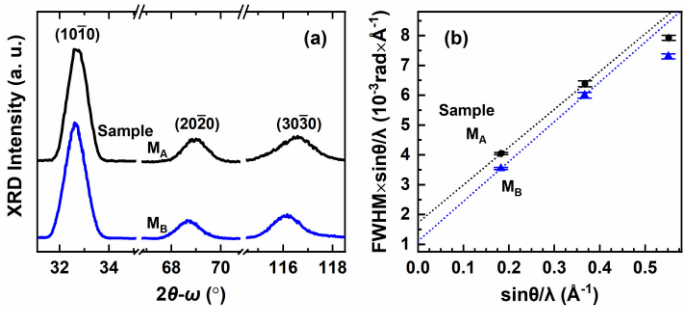

Fig. 3. XRD 2θ-ω curves for (10$\bar{1}$0) and (20$\bar{2}$0)-planes (a) and modified Williamson-Hall plots (b) for samples M_A and M_B.

and the counterparts for *a*-plane GaN is the representative triangle pits [13]. The presence of SPs could certainly result in a rough surface, which is disadvantageous to grow the MQWs structure with flat and abrupt interfaces. It can be seen clearly that the surface morphology of sample M_A was much rougher than that of sample M_B. The SPs density for a 5.3 $\times$ 5.3 μm^2 area was estimated to be 5.47 $\times$ 10^8 cm^{-2} for sample M_A and 3.62 $\times$ 10^8 cm^{-2} for sample M_B. Furthermore, the RMS value for a 5 $\times$ 5 μm^2 detection area was found to be 4.14 nm for sample M_A and 2.15 nm for sample M_B. In other words, the SPs density and RMS value were reduced by 33.8% and 48.1%, respectively due to the optimized dual nitridation. The cross profile TEM image of sample M_B in the MQWs area viewed with a dark-field mode along [10$\bar{1}$0]-axis was demonstrated in Fig. 2(e). It can be observed clearly that the interfaces between the quantum barriers and MQWs were flat and abrupt, indicating a high crystalline quality of MQWs structure for sample M_B. In addition, the bright lines penetrated the MQWs as shown in Fig. 2(e) were assigned to be BSFs, which are presented as bright lines in a dark-field image for nonpolar group-III nitrides [18].

The statistic BSFs density for sample M_B was found to be varied from 1.83 $\times$ 10^5 to 7.52 $\times$ 10^5 cm^{-1} based on different TEM images since the largest observation area was only hundreds of nanometers for a BSFs-resolvable magnification factor. For elimination of this statistics occasionality, the modified Williamson-Hall analysis [19] was introduced to calculate the BSFs densities based on the expression:

$$\omega_{measured} = \Delta\omega_{mosaic} + \frac{\lambda}{2Lsin(\theta_{hkl})}. \quad (1)$$

In this expression, the reciprocal of *L*, 1/*L* represented the BSFs density for the corresponding sample, and the physical significances for other symbols were identical with the reference [19]. Here, in order to achieve a precise calculation, the off-axis XRD 2θ-ω curves were firstly performed along *c*-direction for *m*-plane of samples M_A and M_B as exhibited in Fig. 3(a). The peaks located around 33° and 69° were assigned to the diffraction from (10$\bar{1}$0) and (20$\bar{2}$0)-planes of each nonpolar AlGaN MQWs sample. Subsequently, the X-ray rocking curves (XRCs) were respectively performed for the two diffraction peaks and the corresponding full width at half maximum (FWHM) were obtained. Neglecting the strains in each sample, the modified Williamson-Hall plots for both samples were plotted in Fig. 3(b) and the measured XRD results and further calculated BSFs densities were summarized in Table 1. It was found that the BSFs density was reduced from 3.46 $\times$ 10^5 cm^{-1} for sample M_A to 2.22 $\times$ 10^5 cm^{-1} for sample M_B, a 35.9% decrease due to the optimized dual nitridation process. On the other hand, the FWHM values of on-axis XRCs for sample M_B measured along *c*- and *m*- directions were decreased from 0.633 to 0.565° and from 1.028 to 0.797°, respectively. This result is higher than the reported polar *c*-plane results but close to the nonpolar *a*-plane results [15].

The TDPL and TRPL spectra for samples M_A and M_B were demonstrated in Fig. 4. The IQE, estimated from the ratio of PL integrated intensity at 300 K to that at the lowest temperature, was 18% for sample M_A and 39% for sample M_B. The main peaks located at 281.5 nm for M_A

TABLE 1
2θ Peak Positions and FWHM Values for $(10\bar{1}0)$, $(20\bar{2}0)$ and$(30\bar{3}0)$-Planes Diffraction and Corresponding Calculated BSFs Density for Samples M_A and M_B

Sample	$(10\bar{1}0)$-plane		$(20\bar{2}0)$-plane		$(30\bar{3}0)$-plane		BSFs density (cm^{-1})
	2θ (°)	FWHM (°)	2θ (°)	FWHM (°)	2θ (°)	FWHM (°)	
M_A	32.731	1.267	68.954	0.995	116.520	0.822	$3.46(\pm0.01)\times10^5$
M_B	32.629	1.113	68.712	0.938	116.157	0.759	$2.22(\pm0.03)\times10^5$

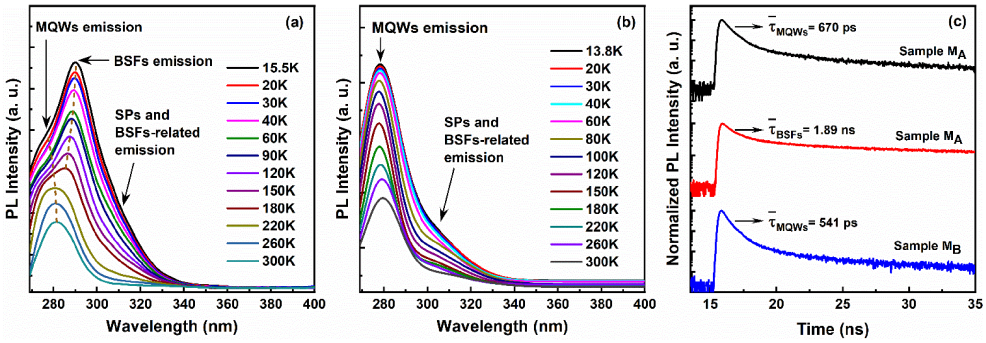

Fig. 4. TDPL spectra measured with the temperature varied from 15.5 to 300 K for sample M_A (a) and from 13.8 to 300 K for sample M_B (b); TRPL decay curves of MQWs and BSFs emission for samples MA and MB measured at 13 K (c). Fig. 4(b) reproduced from Ref. [16], with permission of ACS Publications.

and 279.2 nm for M_B were determined to be the MQWs emission. Unusually, the linewidth of PL spectrum for sample M_A broadened obviously while the temperature decreased from 300 K. When the temperature decreased to 180 K, another emission peak was emerged clearly on the long wavelength side which was located at 285.5 nm. Therefore, the broadened PL linewidth for sample M_A was mainly attributed to the new emerged emission. When the temperature continued to decrease from 180 to 15.5 K, the intensity of this peak was found to be increased significantly and the peak position was gradually redshifted from 285.5 to 290.3 nm. This PL peak was assigned to the BSFs emission [20], [21] and its redshift of peak position was due to the enhanced carrier localization accompanied with the decrease in temperature [21], [22]. Furthermore, at least a third mission peak was inferred to be presented on the right side of BSFs emission based on the optical properties of nonpolar AlGaN materials and the PL spectra line shape. This emission peak contained three hardly resolvable emission channels [23], and both the SPs and BSFs participated in these recombination [22]–[24], thus it was assigned to the SPs and BSFs-related emission. On the other hand, the average lifetime (decreased to a factor of 1/e from maximum value of the decay curve) of MQWs and BSFs emission for both samples were calculated based on the TRPL spectra shown in Fig. 4(c). The average lifetime of MQWs emission were only 670 and 541 ps for samples M_A and M_B, respectively, which are evident faster than the conventional polar counterparts [25]. It was inferred that the extended lifetime of MQWs emission in sample M_A was mainly due to the influence of relatively strong BSFs emission. The achievement of an IQE as high as 39% was attributed to the significantly reduction in radiative lifetime of MQWs emission due to the perfect overlap of the wavefunctions for holes and electrons in nonpolar AlGaN MQWs [10]. This feature can remarkably increase the recombination probability of MQWs emission channel in a nonpolar MQWs structure compared to the polar counterpart. In other words, the recombination probability of other competing channels such as the nonradiative recombination can be significantly decreased. This indicates the high realizability of efficient DUV light sources by means of nonpolar

AlGaN rather than polar counterpart. Moreover, the average lifetime of BSFs emission for sample M_A was 1.89 ns. The exciton transfer process from quantum wells into BSFs, the separation of wavefunctions for electrons and holes in BSFs [26], and the deep localization state [20] are responsible for the extended BSFs emission lifetime.

The intensity of MQWs emission for sample M_A only behaved an obvious increase when the temperature declined from 300 to 180 K while this increase was almost stagnated when the temperature further decreased from 180 to 15.5 K. This fact is remarkably different from the evolution of TDPL spectra for sample M_B. After careful observation of Fig. 4(a), it can be found that the nearly absence of increase in MQWs emission intensity was exactly occurred in the evolution of BSFs emission emerged and then significantly increased. Thus, it was deduced that a majority exciton which were supposed to recombined in quantum wells were trapped and then localized in BSFs. This resulted in the evident increase of BSFs rather than MQWs emission intensity at 180-15.5 K for sample M_A. In fact, the BSFs emission occurred from BSF bunches, acted as the recombination center, rather than from a single one [22]. Therefore, it was inferred that an evident BSFs emission was only observed when the BSFs density was higher than a critical point to form enough BSFs recombination center. Apparently, enough BSFs recombination center was formed in sample M_A due to the relatively high BSFs density. When the temperature increased from 180 K, the BSFs emission of sample M_A was changed from radiative to electron delocalization-related nonradiative recombination [22] and lead to a low IQE. For sample M_B, the BSFs emission was suppressed efficiently due to the evident reduction in BSFs density after the optimized dual nitridation. On the other hand, the SPs and BSFs-related emission for sample M_B was evidently decreased than that for sample M_A. The reduced density of SPs and BSFs, smoother surface, as well as smaller RMS value for sample M_B than these for M_A would certainly result in this situation. Thus, both the effective reduction of BSFs emission and SPs and BSFs-related emission are responsible for the improved IQE. In fact, the preponderant structural defects are BSFs for nonpolar *a*-plane III-nitrides heteroepitaxy grown on *r*-plane sapphire substrate. Most of the BSFs were formed in the initial growth stage, at the interface between epilayer and substrate and were significant influenced by the nucleating layer [18], [27]. After formation, the BSFs could penetrate through the entire epilayer followed the growth sequence as shown in Fig. 2(e). In a word, due to the carefully optimizing of dual nitridation, evident decreases in SPs and BSFs densities as well as RMS value were achieved. This contributed the remarkable improvement of optical properties of sample M_B.

4. Conclusion

The carefully optimized dual nitridation was powerful to improve the structural and optical properties of nonpolar AlGaN-based MQWs. The SPs and BSFs densities were reduced from 5.47×10^8 to 3.62×10^8 cm^{-2} and from 3.46×10^5 to 2.22×10^5 cm^{-1}, respectively, due to the optimized dual nitridation. It was found that the MQWs emission was seriously restricted by the BSFs emission as the BSFs emission was the main competing channels. Thus, the IQE can be significantly improved from 18% to 39% by reducing the BSFs density. Moreover, it was inferred that the carrier recombination probability in nonpolar AlGaN MQWs was remarkably improved compared to that in polar counterpart due to the elimination of QCSE induced the evident decrease in radiative lifetime. This fact means that a high realizability of efficient DUV light sources can be expected by means of nonpolar AlGaN.

References

[1] H. Hirayama *et al.*, "Recent progress and future prospects of algan-based high-efficiency deep-ultraviolet light-emitting diodes," *Jpn. J. Appl. Phys.*, vol. 53, no. 10, 2014, Art. no. 100209.
[2] T.-Y. Seong *et al.*, *III-Nitride Based Light Emitting Diodes and Applications*. Vienna, Austria: Springer, 2013.
[3] C. Huang *et al.*, "Ultraviolet optoelectronic devices based on AlGaN-SiC platform: Towards monolithic photonics integration system," *Nano Energy*, vol. 77, 2020, Art. no. 105149.

[4] Z. Ren *et al.*, "Band engineering of III-nitride-based deep-ultraviolet light-emitting diodes: A review," *J. Phys. D: Appl. Phys.*, vol. 53, no. 7, 2020, Art. no. 073002.
[5] T. Takano *et al.*, "Deep-ultraviolet light-emitting diodes with external quantum efficiency higher than 20% at 275 nm achieved by improving light-extraction efficiency," *Appl. Phys. Exp.*, vol. 10, no. 3, 2017, Art. no. 031002.
[6] H. Sun *et al.*, "Unambiguously enhanced ultraviolet luminescence of AlGaN wavy quantum well structures grown on large misoriented sapphire substrate," *Adv. Funct. Mater.*, vol. 29, no. 48, 2019, Art. no. 1905445.
[7] T. Y. Wang *et al.*, "85% internal quantum efficiency of 280-nm AlGaN multiple quantum wells by defect engineering," *Sci. Rep.*, vol. 7, no. 1, 2017, Art. no. 14422.
[8] M. Kneissl, "UV LED efficiency," Nov. 20, 2018. [Online]. Available: https://www.ifkp.tu-berlin.de/?id = agkneissl, Accessed on: Nov. 9, 2020.
[9] M. Leroux *et al.*, "Quantum confined stark effect due to built-in internal polarization fields in (Al,Ga)N/GaN quantum wells," *Phys. Rev. B*, vol. 58, no. 20, pp. R13371–R13374, 1998.
[10] P. Waltereit *et al.*, "Nitride semiconductors free of electrostatic fields for efficient white light-emitting diodes," *Nature*, vol. 406, no. 6798, pp. 865–868, 2000.
[11] Y. Tsuchiya *et al.*, "Control of p-Type conduction in a-Plane GaN grown on sapphire r-Plane substrate," *Jpn. J. Appl. Phys.*, vol. 44, no. 50, pp. L1516–L1518, 2005.
[12] W. Götz *et al.*, "Activation of acceptors in Mg-doped GaN grown by metalorganic chemical vapor deposition," *Appl. Phys. Lett.*, vol. 68, no. 5, pp. 667–669, 1996.
[13] Q. Sun *et al.*, "Understanding nonpolar GaN growth through kinetic wulff plots," *J. Appl. Phys.*, vol. 104, no. 9, 2008, Art. no. 093523.
[14] J. Zhao *et al.*, "Defects reduction in a-plane AlGaN epi-layers grown on r-plane sapphire substrates by metal organic chemical vapor deposition," *Appl. Phys. Exp.*, vol. 10, no. 1, 2017, Art. no. 011002.
[15] M. Jo *et al.*, "Growth of non-polara-plane AlN on r-plane sapphire," *Jpn. J. Appl. Phys.*, vol. 55, no. 5S, 2016, Art. no. 05FA02.
[16] J. Zhao *et al.*, "High internal quantum efficiency of nonpolar a-Plane algan-Based multiple quantum wells grown on r-Plane sapphire substrate," *ACS Photon.*, vol. 5, no. 5, pp. 1903–1906, 2018.
[17] J. Zhao *et al.*, "Study of dual nitridation processes in growth of non-polar a-plane AlGaN epi-layers," *Mater. Lett.*, vol. 227, pp. 108–111, 2018.
[18] Z. H. Wu *et al.*, "Role of the buffer layer thickness on the formation of basal plane stacking faults in a-plane GaN epitaxy on r-sapphire," *Appl. Phys. Lett.*, vol. 93, no. 1, 2008, Art. no. 011901.
[19] M. B. McLaurin *et al.*, "Basal plane stacking-fault related anisotropy in X-ray rocking curve widths of m-Plane GaN," *Jpn. J. Appl. Phys.*, vol. 47, no. 7, pp. 5429–5431, 2008.
[20] H.-M. Huang *et al.*, "Exciton localization behaviors of basal stacking faults in a-Plane AlGaN alloys," *J. Electrochem. Soc.*, vol. 158, no. 5, 2011, Art. no. H491.
[21] H.-M. Huang *et al.*, "Ultraviolet emission efficiency enhancement of a-plane AlGaN/GaN multiple-quantum-wells with increasing quantum well thickness," *Appl. Phys. Lett.*, vol. 100, no. 26, 2012, Art. no. 261901.
[22] P. P. Paskov *et al.*, "Emission properties of a-plane GaN grown by metal-organic chemical-vapor deposition," *J. Appl. Phys.*, vol. 98, no. 9, 2005, Art. no. 093519.
[23] R. Liu *et al.*, "Luminescence from stacking faults in gallium nitride," *Appl. Phys. Lett.*, vol. 86, no. 2, 2005, Art. no. 021908.
[24] J. Zhao *et al.*, "Improved optical and structural properties of nonpolar a-plane AlGaN epi-layers after Cp2Mg and NH3 treatments," *Opt. Mater. Exp.*, vol. 8, no. 9, pp. 2586–2591, 2018.
[25] F.-F. Xu *et al.*, "High-Performance semi-polar InGaN/GaN green micro light-emitting diodes," *IEEE Photon. J.*, vol. 12, no. 1, Feb. 2020, Art. no. 2500107.
[26] C. Stampfl *et al.*, "Energetics and electronic structure of stacking faults in AlN, GaN, and inN," *Phys. Rev. B*, vol. 57, no. 24, pp. 15052–15055, 1998.
[27] M. J. Kappers *et al.*, "Properties of non-polar a-plane GaN/AlGaN quantum wells," *J. Cryst. Growth*, vol. 310, no. 23, pp. 4983–4986, 2008.